

# Vortex String Formation in Black Hole Superradiance of a Dark Photon with the Higgs Mechanism

William E. East\*

*Perimeter Institute for Theoretical Physics, Waterloo, Ontario N2L 2Y5, Canada.*

Black hole superradiance, which only relies on gravitational interactions, can provide a powerful probe of the existence of ultralight bosons that are weakly coupled to ordinary matter. However, as a boson cloud grows through superradiance, nonlinear effects from interactions with itself or other fields may become important. As a representative example of this, we use nonlinear evolutions to study black hole superradiance of a vector boson that attains a mass, via a coupling to a complex scalar, through the Higgs mechanism. For the cases considered, we find that the superradiant instability can lead to a transient period where the scalar field reaches its symmetry restoration value, leading to the formation of closed vortex strings, the temporary disruption of the exponential growth of the cloud, and an explosive outburst of energy. After the cloud loses sufficient mass, the superradiant growth resumes, and the cycle repeats. Thus, the black hole will be spun down but, potentially, at a much lower rate compared to when nonlinear effects are unimportant, and with the liberated energy going primarily into bosonic radiation instead of gravitational waves.

## I. INTRODUCTION

A number of extensions to the standard model of particle physics postulate the existence of ultralight bosons that are weakly coupled to ordinary matter. This includes the QCD axion [1, 2], the string axiverse [3–6], and dark photons [7–10]. For ultralight bosons with Compton wavelengths comparable to the size of astrophysical black holes, the superradiant instability provides a unique observation probe of the existence of these particles. If such a black hole rotates sufficiently rapidly, it will be unstable to developing a boson cloud [11–13], which may grow to be up to a few percent of the mass of the black hole, spinning down the black hole in the process.

In the absence of other interactions, the saturation of the superradiant instability comes about through gravitational backreaction. As the boson cloud grows, the black hole spins down, and as the rotational frequency of the black hole approaches that of the bosonic cloud, the instability shuts off, and the cloud begins to dissipate through gravitational radiation [14–16]. This gives rise to a number of potential observational signatures. One can constrain the existence of ultralight bosons through measurements of black hole spin inferred from the electromagnetic signatures of accreting systems or gravitational wave observations of merging binaries [17–23]. One can search for a gravitational wave signal of the oscillating boson cloud, either from resolved or a stochastic background of sources [17–19, 24–32]. Finally, one can look for the imprint of a boson cloud on the orbital dynamics of a binary [33–35].

However, if the bosonic field has nonlinear interactions with itself or other matter, these may have important effects on the bosonic cloud before it fully spins down the black hole, possibly suppressing the spin-down and

gravitational wave observational signatures, but also possibly giving rise to new observables [6, 36–38], including through electromagnetic instabilities and plasma effects [39–42]. Compared to the noninteracting case, the role of nonlinear field effects has been less well studied. For the case of the axion, one intriguing suggestion is that, after growing sufficiently large through superradiance, attractive nonlinear interactions will cause a collapse followed by an energetic outburst, a phenomenon known as a bosonova [6]. While numerical simulations [36, 43] suggest this will happen if one starts with a sufficiently large boson cloud, perturbative estimates in the nonrelativistic regime suggest that dissipation through scalar radiation and/or black hole absorption arising from nonlinear interactions will halt the growth of the cloud before a bosonova can occur [38, 44] (cf. Refs. [45, 46]). Part of the challenge in answering this question is that the timescales associated with the scalar field superradiant instability rate are prohibitively long for simulations, while capturing all relevant nonlinear effects with a perturbative analysis is difficult.

In this work, we study black hole superradiance of a vector field that acquires a mass through the Higgs-mechanism, via a coupling to a complex scalar field. This is both a physically motivated mechanism for a vector boson to obtain an ultralight mass [4, 47], and an example of nonlinear field interactions where it is feasible to perform a full nonlinear analysis using numerical simulations. The Abelian Higgs model is also a prototypical model for cosmic strings [48–50], analogous to the vortex lines in superconductors, and, recently, has been studied in the context of dark photon dark matter [51–54].

Here, we find that, as the vector boson cloud grows through superradiance, it drives the scalar field away from its vacuum expectation value (VEV), to smaller magnitudes in the cloud, eventually leading to the formation of vortex strings: one dimensional curves where the scalar vanishes. Thus, black hole superradiance can produce strings, an alternative to cosmic string formation

---

\* weast@perimeterinstitute.ca

channels such as phase transitions in the early universe. These string loops then drive an explosive event, analogous to the bosonova scenario proposed for the axion, where the cloud is disrupted and loses a significant fraction of its energy to radiation (as well as absorption by the black hole). After a brief transient phase, the cloud begins growing again from lower field values, and the cycle repeats.

## II. MODEL

We study an Abelian gauge field in the presence of gravity that obtains a mass through a Higgs-like coupling to a complex scalar  $\Phi$  with the Lagrangian density

$$\mathcal{L} = \frac{R}{16\pi} - \frac{1}{4}F_{ab}F^{ab} - \frac{1}{2}D_a\Phi(D^a\Phi)^* - \frac{1}{2}V(|\Phi|^2) \quad (1)$$

where  $F_{ab} := \nabla_a A_b - \nabla_b A_a$ ,  $D_a := \nabla_a - igA_a$ , and we use units with  $G = c = \hbar = 1$  throughout. For the potential, we take  $V(|\Phi|^2) = (\lambda/2)(|\Phi|^2 - v^2)^2$ . Here  $g$  and  $\lambda$  are coupling constants, and  $v$  is the VEV of the scalar. In this study, we will focus on the regime where non-linear field effects become significant before gravitational backreaction is important and, therefore, will restrict to a fixed black hole spacetime.

Reviewing the arguments of Ref. [37], we can illustrate some features of this system by writing the complex scalar in terms of a phase  $\theta$  and a magnitude fluctuation  $\rho$  around the VEV,  $\Phi = (v + \rho)e^{i\theta}$ , and choosing the unitary gauge where the  $U(1)$  symmetry is used to set the Goldstone boson  $\theta = 0$ . The vector field equation of motion is then  $\nabla_a F^{ab} = \mu^2(1 + \rho/v)^2 A^b$ . Hence, when  $\rho \ll v$ , the vector field will act as a Proca field with mass  $\mu := gv$  and can grow exponentially around a black hole through superradiance. The equation of motion for  $\rho$  is  $\square\rho = V'_{\text{eff}}(\rho)/2$  with  $V_{\text{eff}}(\rho) = V(\rho) + \mu^2(1 + \rho/v)^2 A^2$ , where  $A^2 := A_a A^a$ .

In this work, we will be interested in the case where  $\lambda \gg g^2$ , so that the scalar field is a heavy degree of freedom. When  $A^2 \ll A_c^2 := \lambda v^4/\mu^2$ , the minimum of the effective potential is at  $\rho/v \approx -A^2/(2A_c^2)$ . Thus, as the vector field grows through superradiance, we expect the scalar field to move towards the smaller magnitude. When  $A^2 \geq A_c^2$ , the minimum of the effective potential moves to  $\Phi = 0$ , the field value where the spontaneously broken  $U(1)$  symmetry is restored, and the vector becomes effectively massless. However, approaching this point, we expect strong nonlinear dynamics.

Using a nonrelativistic estimate, we expect the cloud mass at which  $A^2 = A_c^2$  to be  $E/M \sim \alpha^{-4}A_c^2$  where  $M$  is the black hole mass and  $\alpha := \mu M$ . Integrating out the scalar will also give rise to an effective nonlinear term for the vector field  $\nabla_a F^{ab} \approx \mu^2(1 - A^2/A_c^2)A^b$ , which can lead to vector radiation which will carry energy away from the system. In the nonrelativistic and weakly nonlinear regime, we expect the luminosity of this radiation to scale as  $\dot{E}_{\text{rad}} \propto \alpha^6 A_c^{-4}(E/M)^3$  [37]. This should

be compared to the rate at which energy is extracted from the black hole through the superradiant instability  $\dot{E}_{\text{BH}} \propto \alpha^7(E/M)$  [19]. Hence, at  $A^2 = A_c^2$ , the ratio of the radiation and energy extraction rate from the black hole should scale as  $\dot{E}_{\text{BH}}/\dot{E}_{\text{rad}} \propto \alpha^9$ .

In the rest of this work, we will use the Lorenz gauge  $\nabla_a A^a = 0$ , since unitary gauge can be problematic when  $|\Phi| \rightarrow 0$ . However, since in the unitary gauge  $\nabla_a([1 + \rho/v]^2 A^a) = 0$ , and we will choose initial conditions with  $\Phi$  real, we expect the two gauges to approximately agree when  $\rho/v \ll 1$  and  $A^2 \ll A_c^2$ .

## III. METHODOLOGY

We numerically solve the coupled vector-complex scalar equations,

$$D_a D^a \Phi = \frac{dV}{d|\Phi|^2} \Phi, \quad \nabla^a F_{ab} = -g \times \text{Im}(\Phi^* D_b \Phi), \quad (2)$$

where, again,  $g$  is the gauge coupling constant in the Lorenz gauge  $\nabla_a A^a = 0$ , on a fixed black hole spacetime in Kerr-Schild coordinates [55]. The vector field is evolved using the same 3+1 decomposition and constraint damping auxiliary field as in Refs. [56–58]. The complex scalar is evolved as in Ref. [59]. See appendix for more details on the evolution scheme, numerical resolution, and convergence.

The stress-energy tensor of the system is given by

$$T_{ab} = F_{ac}F_b^c - \frac{1}{4}g_{ab}F^{cd}F_{cd} + \frac{1}{2}[D_a\Phi(D_b\Phi)^* + \text{c.c.}] - \frac{1}{2}g_{ab}[|D_c\Phi|^2 + V(|\Phi|^2)]. \quad (3)$$

We will use the fact that our stationary and axisymmetric spacetime has two Killing vectors  $t^a$  and  $\phi^a$ , to define several diagnostic quantities with respect to the stress energy of the system. The energy and angular momentum are, respectively, given by

$$E := \int -T_a^t t^a N \sqrt{\gamma} d^3x, \quad J := \int T_a^\phi \phi^a N \sqrt{\gamma} d^3x, \quad (4)$$

where  $N$  is the lapse and  $\gamma$  is the determinant of the spatial metric. We will evaluate these quantities outside the black hole horizon, but inside some fixed coordinate sphere with size much larger than characteristic boson cloud size (typically we take  $r \geq 50M$ ). Any change in  $E$  and  $J$  will either be due to a flux through the black hole horizon, or due to radiation to the wave zone. We will use  $\dot{E}_{\text{BH}}$  and  $\dot{E}_{\text{rad}}$  to denote the energy flux calculated at the black hole horizon and in the wave zone, respectively. We can also divide the energy (and, similarly, the angular momentum) into contributions from the vector and scalar fields  $E = E_A + E_\Phi$ , corresponding, respectively, to the first and second lines in Eq. 3. Note that the interaction energy for the two fields is, thus, included in  $E_\Phi$ .

In this study, we fix the black hole to have mass  $M$  and a dimensionless spin of  $a = 0.99$ . In this case, we

can always choose to measure  $\Phi$  and  $A_a$  in units of  $v$ , and the relevant dimensionless parameters are  $\alpha := \mu M$  and  $\lambda/g^2 = A_c^2/v^2$ . Because of the associated computational expense, we will be restricted to considering cases where  $\alpha$  is not too small, and considering large, but not extremely large values of  $\lambda/g^2$  (though we will comment on how our results extrapolate to other values). In particular, we consider  $\alpha = 0.4$  and  $\lambda/g^2 = 12.5, 25$ , and  $50$ . We also consider  $\alpha = 0.3$  with  $\lambda/g^2 = 400/9$ . We begin our evolutions near the end of the weakly nonlinear regime with  $\min(|\Phi|/v) > 0.9$ . As described in more detail in the appendix, initial conditions for a superradiantly growing cloud are constructed by first evolving an azimuthally symmetric version of the system for a number of  $e$  folds, and using that as the starting point of the full 3D evolution. We note that, in the absence of nonlinear interactions, the massive vector field instability growth rate is  $\omega_I M = 7 \times 10^{-5}$  and  $2 \times 10^{-4}$  for  $\alpha = 0.3$  and  $0.4$ , respectively [57].

#### IV. RESULTS

Our main result is that we find that, after a sufficiently long period of growth through superradiance, the instability shuts off with the formation of vortex strings, which eventually drive the partial disruption of the boson cloud. In Fig. 1, we see that, as the vector field grows exponentially due to superradiance, the minimum value of  $|\Phi|$  gets closer to zero. In particular, as suggested by the simple argument above,  $\min(|\Phi|/v) \sim 1 - \max(A^2)/(2A_c^2)$  in the weakly nonlinear phase. When  $\min(|\Phi|/v) \approx 0.2$ , there is a strongly dynamical phase where  $|\Phi|$  quickly approaches zero at certain points in the cloud.

This phase is marked by the formation of vortex strings. Within the cloud, a pair of closed vortex-antivortex strings form. The electric field of the cloud drives one outward, while quickly pushing the string with opposite phase winding into the black hole. As illustrated in the snapshots in Fig. 2, for  $\alpha = 0.4$ , one can see that the remaining string (first column) roughly spans a meridian outside of the black hole and has a winding number  $|n| = 1$  (i.e., the phase of  $\Phi$  goes through  $2\pi$  when circling the vortex). It briefly expands, while continuing to rotate (second column), before tension and gravity (coupled with the dissipation of the vector field) cause it to collapse onto the black hole as well. Several short-lived, nonmeridional string loops are excited (third column and top rightmost panel), which then fall into the black hole. Subsequently, as indicated above in Fig. 1,  $|\Phi|/v$  goes above  $\sim 0.9$ , and there are no vortices.

We also show a snapshot from  $\alpha = 0.3$  in Fig. 2. This case is similar to the above, except that the main string has a larger spatial extent, and we also find the formation of additional smaller closed loops (bottom rightmost panel) which, subsequently, collapse.

In the top panel of Fig. 3, we show the energy and angular momentum divided between the vector field con-

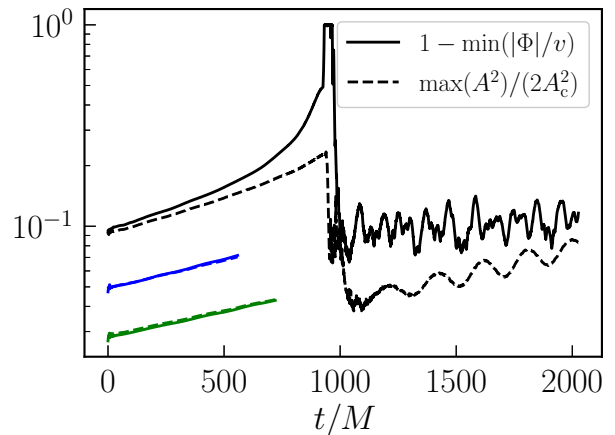


FIG. 1. The displacement of the minimum scalar field value from the VEV (solid curves) and the maximum vector magnitude (dashed curves) as a function of time for cases with  $\alpha = 0.4$  and  $\lambda/g^2 = 25$ . The blue and green curves have the same parameters as the black curves but have initial values for the fields that are, respectively,  $\approx 2$  and  $3 \times$  smaller. At lower field values  $\min(|\Phi|/v) \approx 1 - \max(A^2)/(2A_c^2)$ .

tribution and the scalar field (including the interaction terms with the vector) contribution. As the string vortices form, there is a strong increase in the energy and angular momentum in the scalar sector, with energy and angular momentum being rapidly drained out of the vector sector. During this phase, the flux of energy out of the black hole switches from positive (i.e., superradiance), to strongly negative, as shown in the bottom panel of Fig. 3. In addition, in the lead-up to  $|\Phi|$  approaching zero within the cloud, there is a strong rise in the radiation luminosity, much faster than the  $\dot{E}_{\text{rad}} \propto E^3$  found in the weakly nonlinear phase, with a significant burst during the string vortex phase.

At the end of this strongly dynamical phase, the energy and angular momentum of the cloud have dropped to roughly 30% of their peak values, as shown in the top panel of Fig. 3. The majority of this is due to radiation, with  $\sim 20\%$  of the energy loss (and even less of the angular momentum loss) being due to absorption by the black hole. Shortly afterwards, the flux of energy and angular momentum out of the black hole becomes positive again, and the cloud begins growing exponentially again. Thus, the cycle will repeat, and  $\approx 2000M$  later, there is another disruption event (see Fig. 4). The ratio of energy to angular momentum leading up to, and following the cloud disruption, is roughly the same, and consistent with the linear Proca field frequency  $E/J \approx 0.36M^{-1}$ .

We also compare several different values of  $\lambda$  and  $\mu^2$  in Fig. 4. After scaling out the leading order effect, which is that  $E$  goes as  $A_c^2$ , we see that there is only mild dependence at fixed  $\alpha$  towards smaller peak values, and higher minimum values following disruption of the cloud as  $A_c^2$

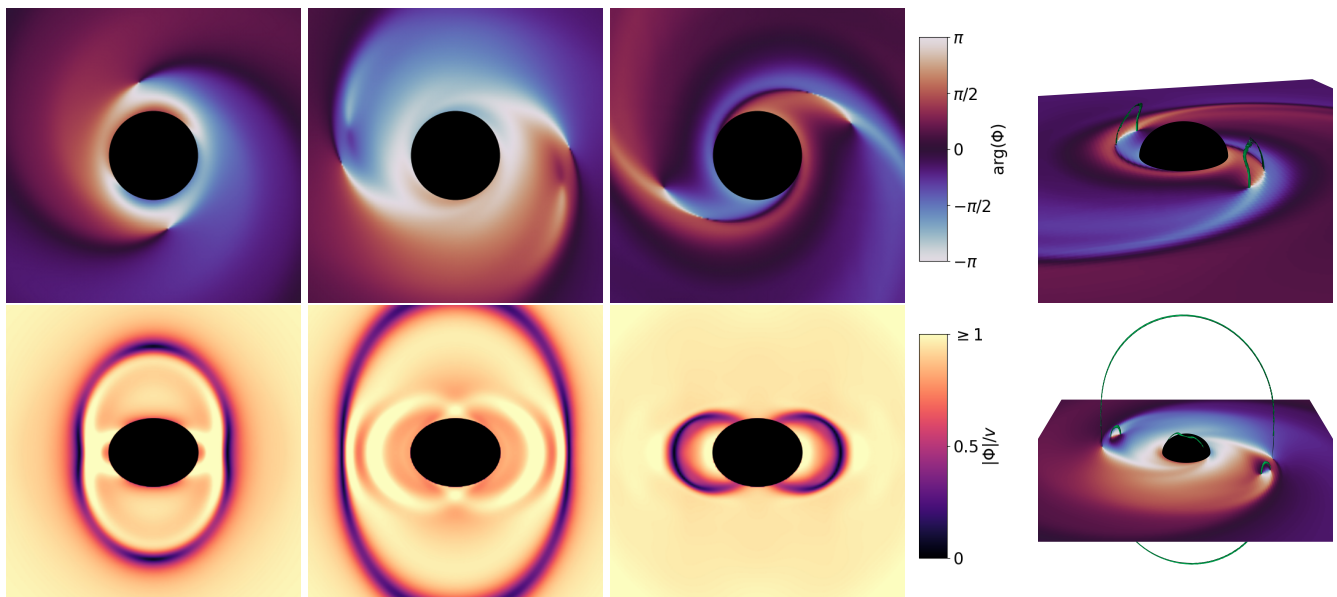


FIG. 2. The three pairs of panels on the left show snapshots of the scalar complex phase  $\arg(\Phi)$  in the equatorial plane of the black hole (top), and the scalar magnitude  $|\Phi|$  in a meridional slice intersecting the black hole and a string at that time, for subsequent times (the second and third are, respectively,  $7M$  and  $24M$  after the first) following vortex formation in a case with  $\alpha = 0.4$  and  $\lambda/g^2 = 25$ . The two rightmost panels show 3D contours of  $|\Phi| \approx 0.08v$  in green, indicating the extent of the strings, as well as the complex phase in the equatorial plane. The top rightmost panel is the same case and same time as the third column, but shows that the nearby pairs of vortices are actually part of the same small loops. (Note that  $|\Phi|$  is small, but does not go to zero on the black hole horizon here.) The bottom rightmost panel is from the case with  $\alpha = 0.3$ . For all cases, the scale can be judged by the size of the black hole horizon (black region), which has proper circumference  $4\pi M$ .

is increased. As an indication of the numerical error, we estimate the error in the peak value of  $E$  for  $\lambda/g^2 = 25$  to be 1% (see the appendix for details). In addition to the cases with  $\alpha = 0.4$ , in this plot, we also show  $\alpha = 0.3$ , which has qualitatively similar behavior. As suggested by the nonrelativistic estimates above, the peak energy (scaled by  $A_2^2$ ) is higher, though only  $\approx 1.7\times$  higher than  $\alpha = 0.4$  and fixed  $M\lambda v^2/g^2$ , which is somewhat less than the  $\alpha^{-4}$  scaling expected in the nonrelativistic limit. For  $\alpha = 0.3$ , when  $\min(|\Phi|) \approx 0.2v$ , which roughly marks the beginning of the strongly nonlinear phase, we find that  $|E_{\text{rad}}/E_{\text{BH}}| \sim 0.01$  (a factor of a few higher than  $\alpha = 0.4$ ). So in this case, the radiation from nonlinear interactions is still subdominant to the rate at which energy is extracted from the black hole through superradiance.

## V. DISCUSSION AND CONCLUSION

We have studied an ultralight boson cloud that grows around a spinning black hole through superradiance, eventually becoming large enough to strongly backreact on the Higgs-like scalar field which gave rise to the vector mass. Restoring physical units for  $\alpha = 0.4$  assuming  $M = 60 M_\odot$  (hence,  $\mu = 9 \times 10^{-13}$  eV), this will happen before the cloud reaches saturation through gravitational interactions (i.e., by spinning down the black hole) when

$v\lambda^{1/4} \lesssim 10$  MeV or, equivalently,  $g\lambda^{-1/4} \gtrsim 10^{-19}$ , where  $\lambda$  is constrained by unitary considerations to not be too large. We showed that, in this case, the boson cloud reaches a maximum energy  $E_{\text{max}}$  and angular momentum  $J_{\text{max}} \approx E_{\text{max}}/\mu$ , with the superradiant growth shutting off as the scalar field reaches its symmetry restoration value at points within the cloud, giving rise to string vortices, and with the majority of the energy of the cloud going into the scalar field. The dynamics of these strings then rapidly dissipate a significant portion of the cloud, with a fraction  $f$  of the angular momentum being radiated away. Afterwards, the superradiant growth of the cloud resumes and will persist until  $E_{\text{max}}$  and  $J_{\text{max}}$  are reached again. Thus, angular momentum will continue to be liberated, but at a slower rate roughly given by  $\sim fJ_{\text{max}}/[\tau \log(1-f)]$ , where  $\tau$  is the superradiant energy and angular momentum  $e$  folding time. For the cases considered here (with  $\alpha = 0.3-0.4$ ), we found  $f \gtrsim 0.5$  and  $E_{\text{max}} \sim 50-80M\lambda v^2/g^2$ . Though we do not consider gravitational backreaction here, if  $\lambda v^2/g^2$  is sufficiently large so that  $E_{\text{max}}$  is non-negligible (but still below the value it would reach in the Proca limit), we may expect a series of gravitational bursts on timescales of  $\tau$ , similar to what was suggested in the bosonova scenario [6, 36, 43]. However, we still expect significant bosonic radiation, in contrast to the Proca limit, where, essentially, all of the rotational energy liberated from the black hole is emitted as gravitational waves.

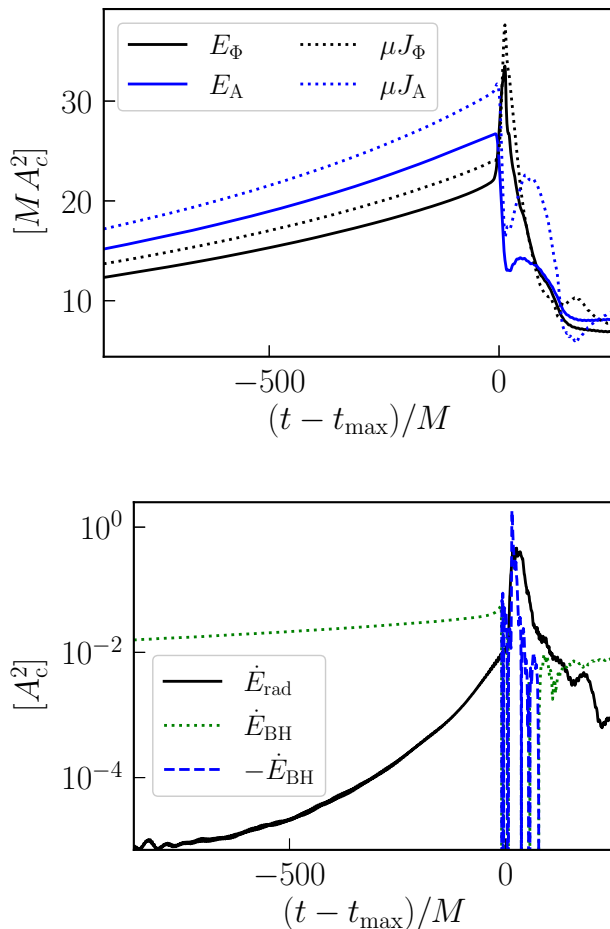


FIG. 3. Top: Energy (solid lines) and angular momentum (dashed lines) as a function of time for  $\alpha = 0.4$  and  $\lambda/g^2 = 25$ . We show the energy and angular momentum contribution from the scalar field, including the interaction term,  $E_\Phi/J_\Phi$ , and the vector field (not including terms involving  $\Phi$ )  $E_A/J_A$  separately. Bottom: The flux of energy extracted ( $\dot{E}_{\text{BH}}$ ) or absorbed ( $-\dot{E}_{\text{BH}}$ ) by the black hole compared to the radiation luminosity for the same case. Here,  $t_{\text{max}}$  is the time when the total energy is maximum.

For the cases considered here, we found that the luminosity of the radiation was subdominant to the energy extraction rate from the black hole due to superradiance in the lead-up to the strongly nonlinear phase. This is consistent with the very recent results of Ref. [60], which studied black hole superradiance of a Proca field with quartic potential and  $\alpha = 0.5$ , finding that the field growth persists until the evolution equations break down (such a system could arise by integrating out the scalar in the Abelian Higgs setup considered here). Based on the relative scalings in the nonrelativistic limit, we expect that, for sufficiently small values of  $\alpha$ , the radiation will become dominant and halt the growth of the cloud before the scalar field is significantly displaced from its

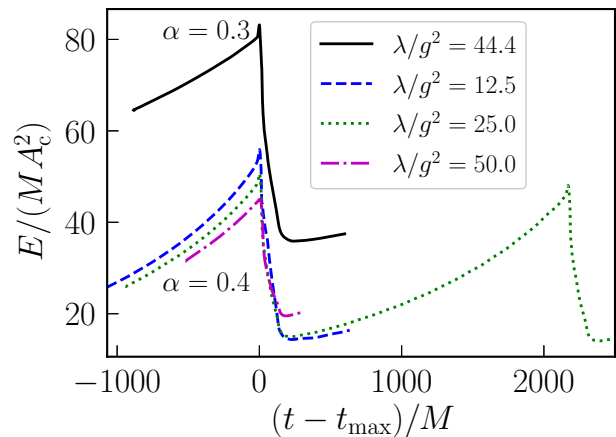


FIG. 4. Total energy as a function of time for cases with  $\alpha = 0.3$  and  $0.4$  and various values of  $\lambda/g^2$ . Here  $t_{\text{max}}$  is the time when the total energy is maximum.

VEV. Though the values of  $\alpha$  considered here were too large to recover the nonrelativistic scaling, we can crudely estimate that this will happen when  $\alpha \lesssim 0.1$ .

We have demonstrated a new formation mechanism, distinct from cosmological scenarios, for forming string loops in the Abelian Higgs model. In this study, for computational reasons, we have also been restricted to relatively modest values of  $\lambda v^2/\mu^2 \leq 50$ , while in general, given that for astrophysical black hole superradiance we have  $\mu \lesssim 10^{-11}$  eV, it is natural to consider scenarios where this ratio is many orders of magnitude larger. In that case, one may expect the characteristic size of the vortex strings to be much smaller compared to the boson cloud size and their density to be larger. An intriguing possibility not covered here is that this gives rise to a network of interacting strings which undergo many reconnections and may lead to the ejection of closed strings from the black hole. This scenario, connections to cosmological scenarios for the dark photon, and possible phenomenological implications when considering a coupling to the standard model are studied in Ref. [54].

## VI. ACKNOWLEDGMENTS

The author thanks Junwu Huang for extensive discussions and Masha Baryakhtar and David Cyncynates for discussion and comments on a draft of this work. The author acknowledges support from an NSERC Discovery grant. This research was supported in part by Perimeter Institute for Theoretical Physics. Research at Perimeter Institute is supported by the Government of Canada through the Department of Innovation, Science and Economic Development Canada and by the Province of Ontario through the Ministry of Colleges and Universities.

This research was enabled by computational resources provided by Calcul Québec (www.calculquebec.ca) and

Compute Canada (www.computecanada.ca), as well as the Symmetry cluster at Perimeter Institute.

- 
- [1] R. Peccei and H. R. Quinn, Phys. Rev. Lett. **38**, 1440 (1977).
- [2] S. Weinberg, Phys. Rev. Lett. **40**, 223 (1978).
- [3] A. Arvanitaki, S. Dimopoulos, S. Dubovsky, N. Kaloper, and J. March-Russell, Phys. Rev. **D81**, 123530 (2010), arXiv:0905.4720 [hep-th].
- [4] M. Goodsell, J. Jaeckel, J. Redondo, and A. Ringwald, JHEP **11**, 027 (2009), arXiv:0909.0515 [hep-ph].
- [5] J. Jaeckel and A. Ringwald, Ann.Rev.Nucl.Part.Sci. **60**, 405 (2010), arXiv:1002.0329 [hep-ph].
- [6] A. Arvanitaki and S. Dubovsky, Phys. Rev. **D83**, 044026 (2011), arXiv:1004.3558 [hep-th].
- [7] B. Holdom, Phys. Lett. **B166**, 196 (1986).
- [8] P. Pani, V. Cardoso, L. Gualtieri, E. Berti, and A. Ishibashi, Phys. Rev. D **86**, 104017 (2012).
- [9] P. W. Graham, J. Mardon, and S. Rajendran, Phys. Rev. D **93**, 103520 (2016), arXiv:1504.02102 [hep-ph].
- [10] P. Agrawal, N. Kitajima, M. Reece, T. Sekiguchi, and F. Takahashi, Phys. Lett. B **801**, 135136 (2020), arXiv:1810.07188 [hep-ph].
- [11] T. Damour, N. Deruelle, and R. Ruffini, Lettere Al Nuovo Cimento Series 2 **15**, 257 (1976).
- [12] S. L. Detweiler, Phys.Rev. **D22**, 2323 (1980).
- [13] T. Zouros and D. Eardley, Annals Phys. **118**, 139 (1979).
- [14] R. Brito, V. Cardoso, and P. Pani, Classical and Quantum Gravity **32**, 134001 (2015).
- [15] W. E. East and F. Pretorius, Phys. Rev. Lett. **119**, 041101 (2017), arXiv:1704.04791 [gr-qc].
- [16] W. E. East, Phys. Rev. Lett. **121**, 131104 (2018), arXiv:1807.00043 [gr-qc].
- [17] A. Arvanitaki, M. Baryakhtar, and X. Huang, Phys. Rev. **D91**, 084011 (2015), arXiv:1411.2263 [hep-ph].
- [18] A. Arvanitaki, M. Baryakhtar, S. Dimopoulos, S. Dubovsky, and R. Lasenby, Phys. Rev. **D95**, 043001 (2017), arXiv:1604.03958 [hep-ph].
- [19] M. Baryakhtar, R. Lasenby, and M. Teo, Phys. Rev. D **96**, 035019 (2017), arXiv:1704.05081 [hep-ph].
- [20] V. Cardoso, Ó. J. Dias, G. S. Hartnett, M. Middleton, P. Pani, and J. E. Santos, Journal of Cosmology and Astroparticle Physics **2018**, 043 (2018).
- [21] R. Roy, S. Vagnozzi, and L. Visinelli, Phys. Rev. D **105**, 083002 (2022), arXiv:2112.06932 [astro-ph.HE].
- [22] K. K. Y. Ng, O. A. Hannuksela, S. Vitale, and T. G. F. Li, Phys. Rev. D **103**, 063010 (2021), arXiv:1908.02312 [gr-qc].
- [23] K. K. Y. Ng, S. Vitale, O. A. Hannuksela, and T. G. F. Li, Phys. Rev. Lett. **126**, 151102 (2021), arXiv:2011.06010 [gr-qc].
- [24] S. D’Antonio, C. Palomba, P. Astone, S. Frasca, G. Intini, I. La Rosa, P. Leaci, S. Mastrogiovanni, A. Miller, F. Muciaccia, O. J. Piccinni, and A. Singhal, Phys. Rev. D **98**, 103017 (2018).
- [25] C. Palomba, S. D’Antonio, P. Astone, S. Frasca, G. Intini, I. La Rosa, P. Leaci, S. Mastrogiovanni, A. L. Miller, F. Muciaccia, O. J. Piccinni, L. Rei, and F. Simula, Phys. Rev. Lett. **123**, 171101 (2019).
- [26] S. J. Zhu, M. Baryakhtar, M. A. Papa, D. Tsuna, N. Kawanaka, and H.-B. Eggenstein, Phys. Rev. D **102**, 063020 (2020).
- [27] M. Isi, L. Sun, R. Brito, and A. Melatos, Phys. Rev. D **99**, 084042 (2019).
- [28] S. Ghosh, E. Berti, R. Brito, and M. Richartz, Phys. Rev. D **99**, 104030 (2019), arXiv:1812.01620 [gr-qc].
- [29] R. Brito, S. Ghosh, E. Barausse, E. Berti, V. Cardoso, I. Dvorkin, A. Klein, and P. Pani, Phys. Rev. Lett. **119**, 131101 (2017), arXiv:1706.05097 [gr-qc].
- [30] R. Brito, S. Ghosh, E. Barausse, E. Berti, V. Cardoso, I. Dvorkin, A. Klein, and P. Pani, Phys. Rev. D **96**, 064050 (2017), arXiv:1706.06311 [gr-qc].
- [31] L. Tsukada, T. Callister, A. Matas, and P. Meyers, Phys. Rev. D **99**, 103015 (2019), arXiv:1812.09622 [astro-ph.HE].
- [32] L. Tsukada, R. Brito, W. E. East, and N. Siemonsen, Phys. Rev. D **103**, 083005 (2021), arXiv:2011.06995 [astro-ph.HE].
- [33] D. Baumann, H. S. Chia, J. Stout, and L. ter Haar, JCAP **12**, 006 (2019), arXiv:1908.10370 [gr-qc].
- [34] D. Baumann, G. Bertone, J. Stout, and G. M. Tomaselli, (2021), arXiv:2112.14777 [gr-qc].
- [35] S. Choudhary, N. Sanchis-Gual, A. Gupta, J. C. Degollado, S. Bose, and J. A. Font, Phys. Rev. D **103**, 044032 (2021), arXiv:2010.00935 [gr-qc].
- [36] H. Yoshino and H. Kodama, Prog. Theor. Phys. **128**, 153 (2012), arXiv:1203.5070 [gr-qc].
- [37] H. Fukuda and K. Nakayama, JHEP **01**, 128 (2020), arXiv:1910.06308 [hep-ph].
- [38] M. Baryakhtar, M. Galanis, R. Lasenby, and O. Simon, Phys. Rev. D **103**, 095019 (2021), arXiv:2011.11646 [hep-ph].
- [39] J. a. G. Rosa and T. W. Kephart, Phys. Rev. Lett. **120**, 231102 (2018), arXiv:1709.06581 [gr-qc].
- [40] S. Sen, Phys. Rev. D **98**, 103012 (2018), arXiv:1805.06471 [hep-ph].
- [41] M. Boskovic, R. Brito, V. Cardoso, T. Ikeda, and H. Witek, Phys. Rev. D **99**, 035006 (2019), arXiv:1811.04945 [gr-qc].
- [42] A. Caputo, S. J. Witte, D. Blas, and P. Pani, Phys. Rev. D **104**, 043006 (2021), arXiv:2102.11280 [hep-ph].
- [43] H. Yoshino and H. Kodama, Class. Quant. Grav. **32**, 214001 (2015), arXiv:1505.00714 [gr-qc].
- [44] A. Gruzinov, (2016), arXiv:1604.06422 [astro-ph.HE].
- [45] H. Omiya, T. Takahashi, and T. Tanaka, PTEP **2021**, 043E02 (2021), arXiv:2012.03473 [gr-qc].
- [46] H. Omiya, T. Takahashi, and T. Tanaka, (2022), arXiv:2201.04382 [gr-qc].
- [47] M. Reece, JHEP **07**, 181 (2019), arXiv:1808.09966 [hep-th].
- [48] H. B. Nielsen and P. Olesen, Nuclear Physics B **61**, 45 (1973).
- [49] M. B. Hindmarsh and T. W. B. Kibble, Rept. Prog. Phys. **58**, 477 (1995), arXiv:hep-ph/9411342.
- [50] A. Vilenkin and E. P. S. Shellard, *Cosmic Strings and Other Topological Defects* (2000).

- [51] A. J. Long and L.-T. Wang, Phys. Rev. D **99**, 063529 (2019), arXiv:1901.03312 [hep-ph].
- [52] M. Redi and A. Tesi, (2022), arXiv:2204.14274 [hep-ph].
- [53] T. Sato, F. Takahashi, and M. Yamada, (2022), arXiv:2204.11896 [hep-ph].
- [54] W. E. East and J. Huang, (2022), arXiv:2206.12432 [hep-ph].
- [55] R. P. Kerr and A. Schild, in *IV Centenario Della Nascita di Galileo Galilei* (1965) p. 222.
- [56] M. Zilhão, H. Witek, and V. Cardoso, Class. Quant. Grav. **32**, 234003 (2015), arXiv:1505.00797 [gr-qc].
- [57] W. E. East, Phys. Rev. **D96**, 024004 (2017), arXiv:1705.01544 [gr-qc].
- [58] T. Helfer, J. C. Aurrekoetxea, and E. A. Lim, Phys. Rev. D **99**, 104028 (2019), arXiv:1808.06678 [gr-qc].
- [59] N. Siemonsen and W. E. East, Phys. Rev. D **103**, 044022 (2021), arXiv:2011.08247 [gr-qc].
- [60] K. Clough, T. Helfer, H. Witek, and E. Berti, (2022), arXiv:2204.10868 [gr-qc].
- [61] A. Dedner, F. Kemm, D. Kröner, C. D. Munz, T. Schnitzer, and M. Wenberg, Journal of Computational Physics **175**, 645 (2002).
- [62] F. Pretorius, Class. Quant. Grav. **22**, 425 (2005), arXiv:gr-qc/0407110 [gr-qc].

## Appendix A: Evolution Equations

We evolve the coupled Abelian Higgs equations for the vector and complex scalar field (Eq. 2) on a black hole background. These equations have a  $U(1)$  symmetry and are invariant under the gauge transformation

$$\Phi \rightarrow \Phi e^{-i\theta}, \quad A^a \rightarrow A^a - \frac{1}{g} \nabla^a \theta. \quad (\text{A1})$$

In unitary gauge,  $\Phi$  is chosen to be real. However, this gauge can be problematic when vortices form, and we instead evolve the equations using the Lorenz gauge  $\nabla_a A^a = 0$ .

For the evolution of the scalar field, we directly evolve the real and imaginary components of  $\Phi = \Phi_R + i\Phi_I$  and  $\partial_t \Phi$  according to

$$\square \Phi = ig\Phi \nabla_a A^a + 2igA^a \nabla_a \Phi + g^2 A_a A^a \Phi + \lambda(|\Phi|^2 - v^2)\Phi. \quad (\text{A2})$$

Choosing the Lorenz gauge, the first term on the right hand side vanishes.

As in Refs. [56–58], to evolve the vector field we decompose into time and spatial components:

$$A_a = \chi_a + n_a \chi, \quad (\text{A3})$$

where  $n_a$  is the unit normal to slices of constant coordinate time, and introduce an electric field

$$E_i = \gamma_i^a F_{ab} n^b, \quad (\text{A4})$$

where  $\gamma_b^a = \delta_b^a + n^a n_b$  is the spatial projection operator. Here, and in the following, the indices  $\{i, j, k, \dots\}$  are spatial indices that run from 1 to 3, as opposed to the spacetime indices  $\{a, b, c, \dots\}$ , which run from 0

to 3. Following Refs. [56, 61], we also introduce an auxiliary field  $Z$  designed to damp away violations of the constraint. In terms of these variables, the evolution equations are

$$N^{-1}(\partial_t - \mathcal{L}_\beta)\chi_i = -E_i - \partial_i \chi - \chi \partial_i \log N, \quad (\text{A5})$$

$$N^{-1}(\partial_t - \mathcal{L}_\beta)\chi = K\chi - \mathcal{D}_i \chi^i - \chi^i \partial_i \log N - Z, \quad (\text{A6})$$

$$N^{-1}(\partial_t - \mathcal{L}_\beta)E^i = KE^i + \mathcal{D}^i Z + \epsilon^{ijk} \mathcal{D}_j B_k - \epsilon^{ijk} B_j \partial_k \log N + g^2 |\Phi|^2 \chi^i - g(\Phi_R \partial^i \Phi_I - \Phi_I \partial^i \Phi_R), \quad (\text{A7})$$

$$N^{-1}(\partial_t - \mathcal{L}_\beta)Z = -\sigma Z + \mathcal{D}_i E^i + g^2 |\Phi|^2 \chi + gN^{-1} \Phi_R (\partial_t - \beta^i \partial_i) \Phi_I - gN^{-1} \Phi_I (\partial_t - \beta^i \partial_i) \Phi_R, \quad (\text{A8})$$

where  $N$  and  $\beta^i$  are the lapse and shift, respectively,  $K$  is the trace of the extrinsic curvature,  $\mathcal{D}_i$  is the covariant derivative associated with the spatial metric,  $\epsilon_{ijk}$  is the spatial totally antisymmetric tensor, and  $B^i = \epsilon^{ijk} \mathcal{D}_j \chi_k$  is the magnetic field. The coupled vector-scalar fields are evolved on a black hole spacetime in Kerr-Schild coordinates [55]. In the numerical evolution scheme, spatial derivatives are calculated with standard fourth-order finite difference stencils and the time evolution is carried out with fourth-order Runge-Kutta, though the interpolation in time for mesh refinement boundaries is only third-order accurate [57, 59].

## Appendix B: Initial Conditions

We construct initial data for our evolutions by first evolving an approximate symmetry-reduced version of our model. In this approximate version, we assume that the vector field has an  $m = 1$  azimuthal symmetry, and that the scalar field is real (i.e. we take unitary gauge) and has an  $m = 0$  azimuthal symmetry. This means the Lorenz gauge condition is replaced by  $\nabla_a A^a = -2A^a \nabla_a \log \Phi$ . In order for this to be consistent, we also have to modify the scalar equation of motion Eq. A2 by replacing the  $g^2 A^2 \Phi$  term by its azimuthally-averaged value. Similar to Ref. [57], we choose an initial vector perturbation and then evolve the symmetry-reduced system for a number of e-folding times until the solution is dominated by the fastest growing superradiantly unstable mode. The result is then taken as initial conditions for evolving the full system without symmetry assumptions. There is a short initial transient due to the fact that the scalar field must relax to its non-axisymmetric and Lorenz gauge value. However, as can be seen from, e.g., Fig. 1, this is mild as we consider initial conditions with  $\min(|\Phi|/v) > 0.9$ .

## Appendix C: Numerical Convergence

For our computational domain, we use six cubic levels of mesh refinement centered on the black hole. The finest

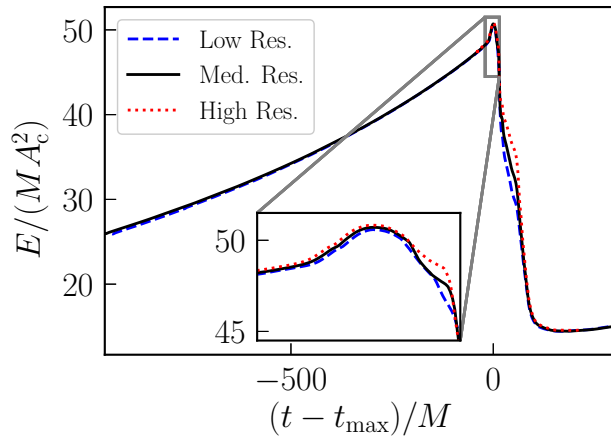


FIG. 5. Energy as a function of time for  $\alpha = 0.4$ ,  $\lambda/g^2 = 25$ , and three numerical resolutions. The inset shows a zoom-in around the time the energy reaches a maximum.

level has a linear dimension of  $L \approx 5M$ , and each subsequent coarser level has a linear dimension and grid spacing that is twice as large. We use compactified coordinates which extend to spatial infinity following Ref. [62]. For our default resolution, the finest level has a grid spacing of  $dx \approx 0.1\lambda^{-1/2}v^{-1}$ .

For the case with  $\alpha = 0.4$  and  $\lambda/g^2 = 25$ , we perform a resolution study with grid spacing that is  $0.75\times$  and  $0.5\times$  as large. For computational expediency, for the highest resolution we begin  $\sim 50M$  before the system achieves peak energy, using the next highest resolution to set initial conditions. We show the total energy as a function of time for the three resolutions in Fig. 5. Using the three resolutions, we estimate that the lowest resolution (which is the minimum resolution for all the results in the main text) underestimates the maximum energy by  $\approx 1\%$ . (The Richardson extrapolation of this diagnostic quantity is consistent with first order convergence, likely due to the discrete way points inside the black hole horizon are excluded when numerically integrating the total energy.)